

## **Utilizing Satellite Imagery to Map Lake Surface Temperature and Explore its Effect on Evaporation Rate**

**Mohamed Elshabi<sup>1</sup>, Mohamed Hussein<sup>1\*</sup>, and Mohamed Fekry<sup>1</sup>**

<sup>1</sup>*Civil Engineering Department, Faculty of Engineering, Aswan University, Aswan 81542, Egypt.*

Received: 14 / 10 / 2024

Accepted: 5 / 1 / 2025

© Unit of Environmental Studies and Development, Aswan University

### **Abstract:**

This study aims to map the Lake Surface Water Temperature (LSWT) for the northern part of Aswan High Dam Lake (AHDL) within the years 2018, 2019, and 2020; and detect the effect of the estimated LSWT on the evaporation rate. To achieve these objectives, firstly, the LSWT maps were created from the Landsat-8 satellite images, a widely and conventional used method. Moreover, the LSWT maps were also generated by Sentinel-3 Sea and Land Surface Temperature Radiometer (Sentinel-3/SLSTR) satellite images. The created temperature maps by Landsat-8 were used to assess the ones produced by Sentinel-3. Then the relationship between the Sentinel-3 derived LSWT and the estimated evaporation rate, provided by floating hydro-meteorological stations within AHDL and reported by annual reports of the Ministry of Water Resources and Irrigation (MWRI), was determined. After assessing, it was found that the convergence percentage between the estimated temperature values by the Sentinel-3 and those estimated by Landsat-8 (the reference values) ranges from 1.00% to 4.71%, which indicates that the estimated temperature values from both satellite images are very close. Therefore, it is possible to rely on the results of the created temperature maps for the study area by Sentinel-3. Additionally, the study revealed a direct relationship between the evaporation rate and the LSWT estimated by Sentinel-3 within the same year. However, the results demonstrated that changes in the evaporation rate vary from year to year, indicating that LSWT is not the sole factor influencing.

**Keywords:** AHDL, LSWT, Sentinel-3/SLSTR, Landsat-8, Evaporation rate.

### **1- Introduction**

LSWT is an important indicator of lake biogeochemistry and hydrology. Therefore, accurate water surface temperature (WST) data must be obtained to study the hydrologic cycle of lakes (Reinart and Reinhold, 2008). Furthermore, realistic LSWT data can also be used to estimate and characterize evaporation from lakes. Measurements of evaporation are therefore important for water budget estimation and proper management of lakes (Lenters et al., 2005).

---

**Corresponding author\*:** E-mail address: [cemh500@gmail.com](mailto:cemh500@gmail.com)

The majority of researches still depend on the use of in-situ measured temperature data, which are relatively time-consuming and labor-intensive, which make it difficult to obtain water temperature information over an extensive area. RS data not only enhances efficiency in monitoring of WST by providing additional water temperature reflection data, but it also helps in providing reliable water surface temperature data and saving manpower and material resources (Kong et al., 2024). Moreover, remote sensing offers an efficient approach for LSWT estimation; as it gives a continuous global record of WST and provides significant information on global climate change (Oesch et al., 2008). Several remote sensing sensors provide data about Earth's surface temperature. Therefore, it plays an important role in the environmental researches and management (Steissberg et al., 2005; Langer et al., 2010). Examples of estimating LSWT from RS data include the following: Layden et al., (2015) estimated LSWT for 246 large lakes using multi-channel imaging radiometers over the period from 1991 to 2011. Alcantara et al., (2010) analyzed more than 1,200 land surface temperature images from Moderate Resolution imaging spectroradiometer (MODIS) to capture WST in the Itumbiara hydroelectric reservoir in Brazil. Also, sea surface temperature product via the MODIS has been utilized in studying lakes Vättern and Vänern in Brazil by Reinart and Reinhold, (2008). Furthermore, several studies investigated on the influence of meteorological changes on lakes' evaporation; for example, not limited to, Meng et al., 2020; Gianniou and Antonopoulos, 2007; Xiao et al., 2020; and Lazhu et al., 2016. Evaporation was significantly influenced by temperature more than solar radiation within Lake Erhai in China (Meng et al., 2020). The study of Lake Vegoritis in Greece, demonstrated that the atmospheric radiation had a greater effect on the evaporation than solar radiation (Gianniou and Antonopoulos, 2007). Atmospheric and solar radiation had a great influence on Lake Taihu of China during the evaporation (Xiao et al., 2020). Moreover, the effects of air temperature, atmospheric radiation, and solar radiation on evaporation from Lake Nam Co in China were detected (Lazhu et al., 2016). Although these previous studies quantified the effect of meteorological changes on evaporation from lakes, analysis of the results are limited due to the lack of information about the variables that related to evaporation process (e.g., lake surface temperature). In Egypt, for AHDL; the water balance highly depends on evaporation, which in turn will lead to reducing the availability of water amount in this lake. Many studies have investigated the evaporation from the AHDL (Abou El-Magd and Ali, 2012; Mohamed et al., 2010). Some research has been conducted to evaluate the lake's surface water temperature (Agrama, 2011; Hassan, 2013). Ebaid and Ismail (2010) studied closing some AHDL khours to reduce the surface area affected by evaporation. For Lake Nasser (the northern part of AHDL), the average annual evaporation loss is predicted to rise by about 0.47 km<sup>3</sup>, 0.88 km<sup>3</sup> and 1.66 km<sup>3</sup> within the years 2030, 2050 and 2100, respectively (Elba et al., 2017). Bates et al. (2008) observed that the evaporation loss from Lake Nasser, which represents about 20 km<sup>3</sup> annually, will increase gradually. Although many previous studies estimated the evaporation losses and the evaporation rate from AHDL, which influenced by global warming and temperatures rise, few previous studies analyzed the effect of the lake surface temperature on its evaporation rate (EL-Mekawy et al., 2018; El-Moattassem et al., 1993). Obtaining the water temperature using data from the Landsat 8 remote sensing satellite has been ongoing for many years, which are relatively taking much time and needs to a complicated processing and many formulas to estimate LSWT, making it challenging to acquire water temperature information over large areas. Using Sentinel-3/SLSTR Satellite data will overcome the above challenges, generating reliable surface water temperature data for the AHDL with an easy and fast processing by using very few formulas specially in SLSTR Level 2 products (Garcia, 2021). The purpose of this study is to generate the LSWT maps for a part from AHDL using RS data, to explore the effect of the LSWT on the

estimated evaporation rate within AHDL. This study is considered an attempt to use Sentinel-3/SLSTR for mapping the lake surface temperature distribution and comparing the results with those of Landsat- 8 data. Finally, the impact of LSWT on the rate of evaporation loss from AHDL has been investigated. It is envisioned that the outcome of this study may imply some significance for researches related to LSWT and its influence on evaporative loss, which will be of utmost importance for the future sustainable management of lakes.

## 2-Materials and Methods

### The Study Area

AHDL, is a large artificial lake that was created by building the High Dam on the Nile River in Aswan, Egypt. This lake is about 479 km long and 16 km wide at its widest portion, near the Tropic of Cancer (Omran and Negm, 2019). The present study focuses on a part of AHDL (the study area) that extends between latitudes  $22^{\circ} 30' N$  and  $24^{\circ} 00' N$  and longitudes  $32^{\circ} 20' E$  and  $33^{\circ} 20' E$ , as shown in Figure 1. The study area, was chosen because of the availability of the used remotely sensed data in the same dates within the studied years for this part of the AHDL only.

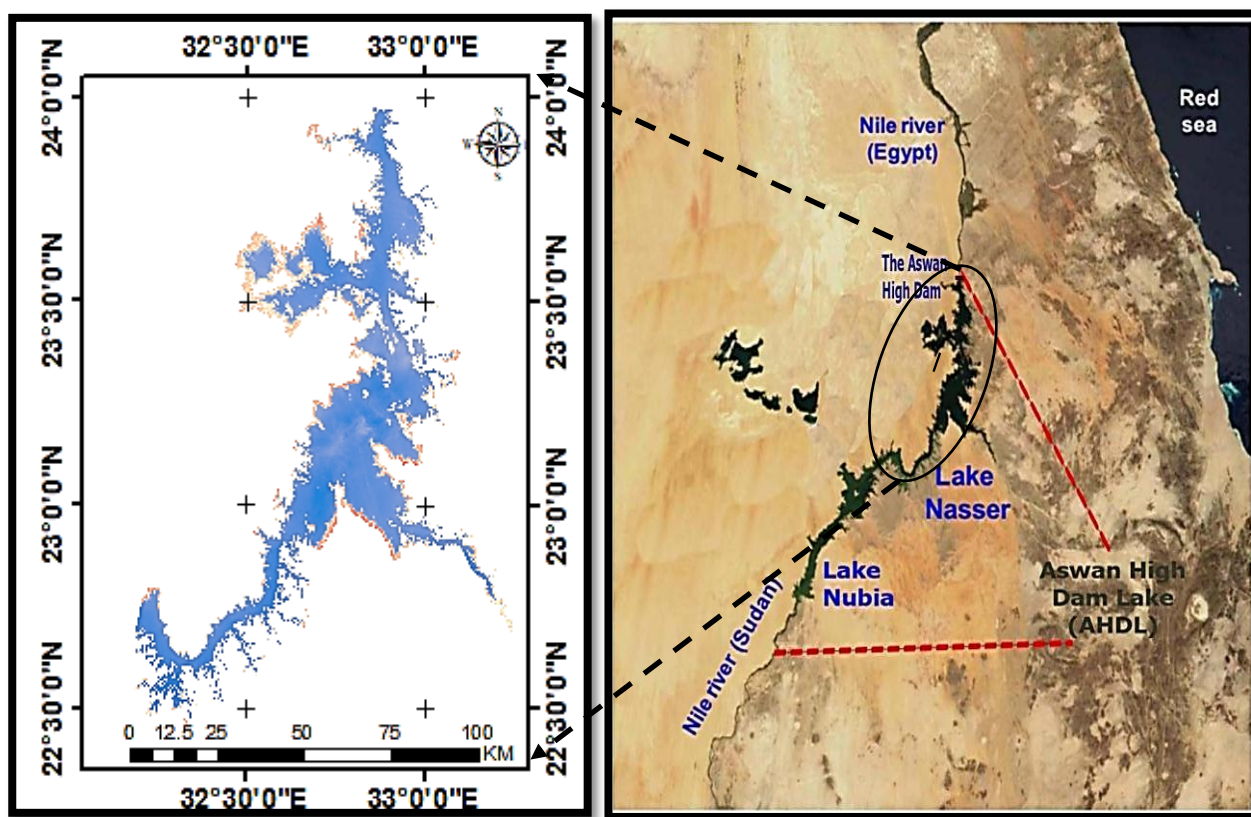


Fig. 1 The location of the study area

### 2.1 Collected data

The collected data to achieve the objectives of the present study include the available remote sensing and the evaporation rate data. These data are specified in the following subsections:

#### 2.2.1 Remote Sensing Data

- The study was conducted in the three months of March, April and May in the years

2018, 2019, and 2020. These years were chosen because of the availability of both Landsat 8 images and Sentinel-3/SLSTR images that cover the same part of AHDL which represent the chosen study area, in the same dates for each year.

- Landsat 8 images, that cover the study area for the periods of study, have been uploaded from USGS site:(<https://earthexplorer.usgs.gov/>). The specifications of Landsat 8 images are shown in Table 1.
- The Sentinel-3 images, that cover the study area for the studied periods, have been uploaded from site: <https://scihub.copernicus.eu/dhus/#/home>. The specifications of Sentinel-3 images are indicated in Table2.

### 2.2.2 Data about the evaporation rate

The evaporation rate from the AHDL were obtained for the studied periods. These data were provided by floating hydro-meteorological stations within AHDL and reported by the annual reports of MWRI (MWRI, 2022).

**Table 1.** Spectral bands of Landsat 8 images

Band name	OLI band number	MSI band number	HLS band code name	Wavelength (micrometers)	Resolution (meters)
Coastal Aerosol	-	1	CA	0.43 - 0.45	60
Blue	2	2	BLUE	0.45 - 0.51	30
Green	3	3	GREEN	0.53 - 0.59	30
Red	4	4	RED	0.64 - 0.67	30
Red-Edge 1	-	5	RE1	0.69 - 0.71	20
Red-Edge 2	-	6	RE2	0.73 - 0.75	20
Red-Edge 3	-	7	RE3	0.77 - 0.79	20
NIR Narrow	5	8A	NIR1	0.85 - 0.88	30
NIR Broad	-	8	NIR2	0.78 - 0.88	10
SWIR 1	6	11	SWIR1	1.56 - 1.66	30
SWIR 2	7	12	SWIR2	2.11 - 2.29	30
Panchromatic	8	-	PAN	0.50 - 0.68	15
Cirrus	9	10	CIRRUS	1.36 - 1.38	30
TIRS 1	10	-	TIRS1	10.60 - 11.19	100
TIRS 2	11	-	TIRS2	11.50 - 12.51	100

**Table 2.** Spectral bands of Sentinel-3 images

Band	$\lambda$ center (nm)	Width (nm)	Function
Oa01	400	15	Aerosol correction, improved water constituent retrieval
Oa02	412.5	10	Yellow substance and detrital pigments (turbidity)
Oa03	442.5	10	Chlorophyll absorption maximum, biogeochemistry, vegetation
Oa04	490	10	High Chlorophyll
Oa05	510	10	Chlorophyll, sediment, turbidity, red tide
Oa06	560	10	Chlorophyll reference (Chlorophyll minimum)
Oa07	620	10	Sediment loading
Oa08	665	10	Chlorophyll (2nd Chlorophyll absorption maximum), sediment, yellow substance/vegetation
Oa09	673.75	7.5	For improved fluorescence retrieval and to better account for smile together with the bands 665 and 680 nm
Oa10	681.25	7.5	Chlorophyll fluorescence peak, red edge
Oa11	708.75	10	Chlorophyll fluorescence baseline, red edge transition
Oa12	753.75	7.5	O2 absorption/clouds, vegetation
Oa13	761.25	2.5	O2 absorption band/aerosol correction
Oa14	764.375	3.75	Atmospheric correction
Oa15	767.5	2.5	O2A used for cloud top pressure, fluorescence over land
Oa16	778.75	15	Atmos. corr./aerosol corr.
Oa17	865	20	Atmospheric correction/aerosol correction, clouds, pixel co-registration
Oa18	885	10	Water vapor absorption reference band. Common reference band with SLSTR instrument. Vegetation monitoring
Oa19	900	10	Water vapor absorption/vegetation monitoring (maximum reflectance)
Oa20	940	20	Water vapor absorption, Atmospheric correction/aerosol correction
Oa21	1020	40	Atmospheric correction/aerosol correction

## 2.2 Methodology

To achieve the goals of the present research, the tasks presented in Figure 2 are conducted.

### 2.3.1 Estimation of Lake Surface Water Temperature using Landsat-8 satellite images

The inverse of the Planck function, which is considered one of the most accurate methods for estimating LST using Landsat-8 satellite images (Chang and Li, 1996), was used to evaluate lake surface water temperature values extracted from Sentinel-3/SLSTR satellite images as shown in Figure 2. The following procedures were implemented for estimating LSWT by the Landsat-8 images.

- **Conversion to Top-of-Atmosphere (TOA) Radiance**

Conversion to (TOA) radiance includes transforming satellite sensor data to radiance values which representing the energy received at the top of the Earth's atmosphere. This process is highly significant for RS applications, including weather forecasting and climate monitoring (Estévez et al., 2021). The used formula for calculating the TOA radiance from the corrected radiance values is:

$$L(\lambda) = ML \times Band\ 10 + AL - Oi\ (1)$$

Where:

$L(\lambda)$ : TOA spectral radiance

ML: Radiance multiplicative band (from MTL txt)  
 AL: Radiance add band #10 (from MTL txt)  
 Oi: correction value (for Landsat 8 Band#10 its = 0.29)

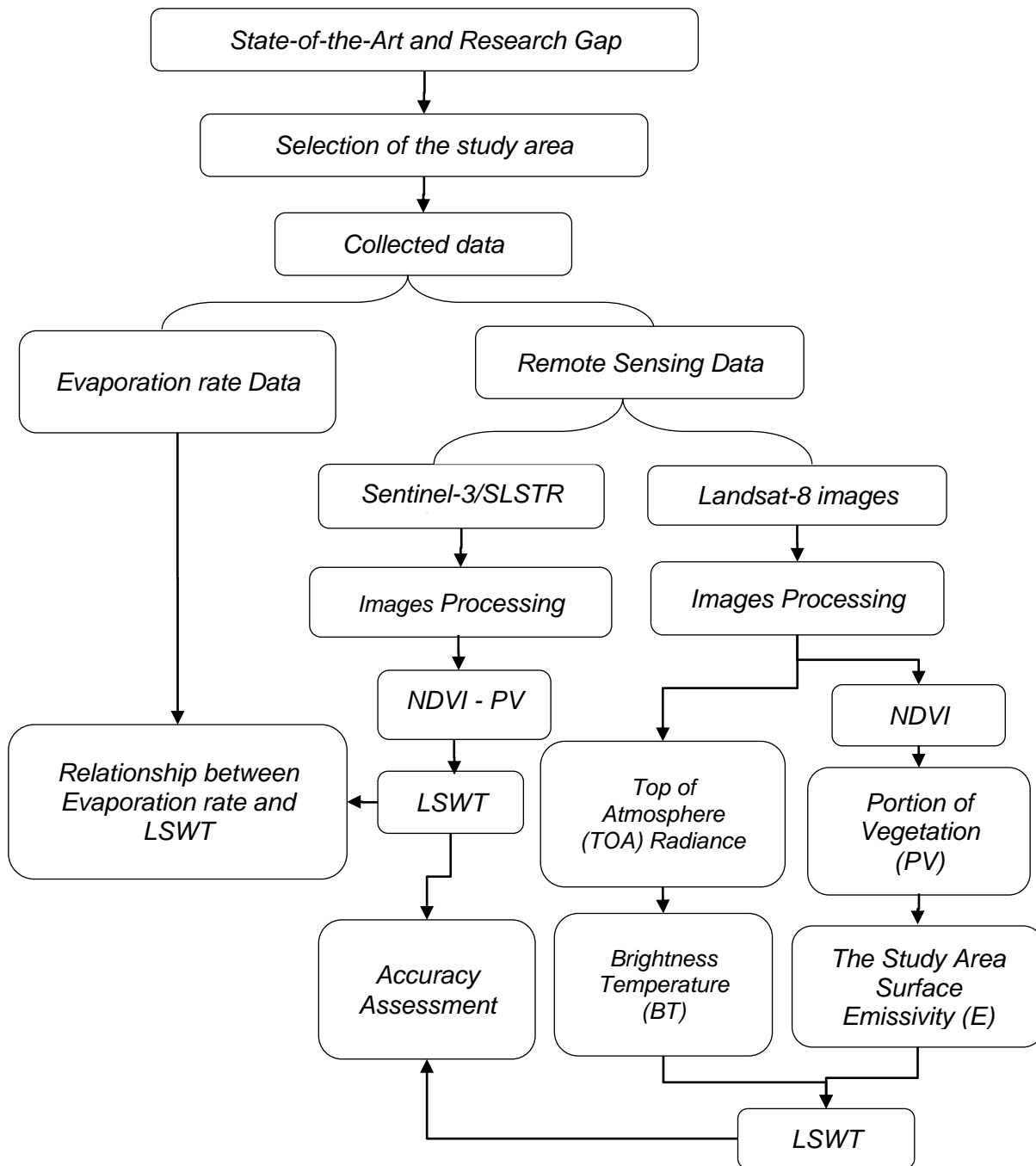


**Fig. 2** Flowchart of the procedures adopted in this research to achieve its objectives

### Conversion of Top-of-Atmosphere to Brightness Temperature (BT)

The conversion of the TOA spectral radiance to the BT is a main aspect in RS applications. This transformation depends on the relationship between the released surface temperature obtained by the Planck's function, and the measured radiation by the satellite sensors (Choung

et al., 2018). The following formula is used to convert TOA to BT:

$$BT = \frac{K2}{\ln \left( \frac{k1}{L(\lambda) + 1} \right) - 273.15} \quad (2)$$

Where:

BT: Top of Atmosphere brightness temperature Co

L(λ): TOA spectral radiance

K1: K1 constant for band#10 (from MTL txt)

K2: Calibration constant specific to Band#10, also retrieved from the MTL.txt file.

### Computation of Normalized Difference Vegetation Index (NDVI)

NDVI is an important index for evaluating vegetation density and growth by RS data (Huang et al., 2021). It depends on the variance between the near-infrared light, which reflects vegetation strongly, and the absorbed red light by vegetation. The NDVI is expressed by the following formula:

$$NDVI = \frac{NIR - RED}{NIR + RED} \quad (3)$$

Where: NIR: band#5 & RED: band#4

- **Computation of Portion of Vegetation (PV)**

The PV, also known as fractional vegetation cover, represents the fraction of an area covered by vegetation. This index has been used in widely applied in the agricultural and environmental areas; especially for land surface temperature estimation and ecosystem monitoring (Zhao and Qu, 2024). The PV formula is as below:

$$PV = \left( \frac{NDVI - NDVI \min}{NDVI \max - NDVI \min} \right)^2 \quad (4)$$

Where:

PV: Portion of Vegetation & NDVI: values of NDVI image3

NDVI max/min: Max & Min values of NDVI image

- **Computation of Lake Surface Emissivity**

The emissivity lake surface refers to the lake surface ability of emitting thermal radiation. This procedure is important for estimating surface temperatures precisely and for a deep understanding the energy exchange among lakes and their surrounding atmosphere (Xu et al., 2023). Lake Surface Emissivity is calculated by the following formula:

$$E = 0.004 * PV + 0.986 \quad (5)$$

Where: E: Lake Surface Emissivity

- **Computation of Lake Surface Water Temperature (LSWT)**

Estimation of LSWT is crucial process for environmental monitoring (Zhu et al., 2020). The LSWT values are attained by the following formula:

$$LSWT = \frac{BT}{1 + \left( \lambda * \frac{\lambda * BT}{C2} \right) * \ln(E)} \quad (6)$$

Where:

BT: Top of Atmosphere brightness temperature Co

$\lambda$ : Wavelength of emitted radiance

for Landsat8 Band#10  $\lambda= 10.8$  and for Band#11  $\lambda=12$

E : Land Surface Emissivity

$C2 = h*c/s$              $C2= 14388$  mK

h: Plank's constant =  $6.626 * 10^{-34}$  mK

s: Boltzmann constant =  $1.38*10^{-23}$  JK

c: velocity of light =  $2.998*10^8$  m/s

### **2.3.2 Estimation of LSWT by Sentinel-3/SLSTR satellite images**

Toolbox S3TBX quickly and directly performed applying the atmospheric correction of the Sentinel-3/SLSTR bands under open-source software environment Sentinel Application Platform (SNAP). Then, NDVI and PV values were derived by applying calculation algorithms developed and applied by the ESA on official SLSTR Level 2 products (Garcia, 2021). Finally, the Copernicus Global Land Service including data collected from ENVISAT AATSR and Sentinel- 3/SLSTR sensors was used as a satellite-based LSWT product (Obertegger and Flaim, 2021).

### **2.3.3 Accuracy Assessment**

It's important to validate the Sentinel-3/SLSTR satellite-derived temperatures with the Landsat-8 satellite-derived temperatures (reference values) to ensure accuracy. In this context, the accuracy of LSWT values retrieved from Sentinel-3/SLSTR satellite images was assessed by comparing them with temperature values obtained using the inverse of the Planck function from Landsat-8 images.

### **2.3.4 Relationship between Changes in Evaporation Rate and LSWT.**

After evaluating LSWT, the relationship between changes in evaporation rate and LSWT was explored to facilitate a better understanding its effect on evaporation rate.

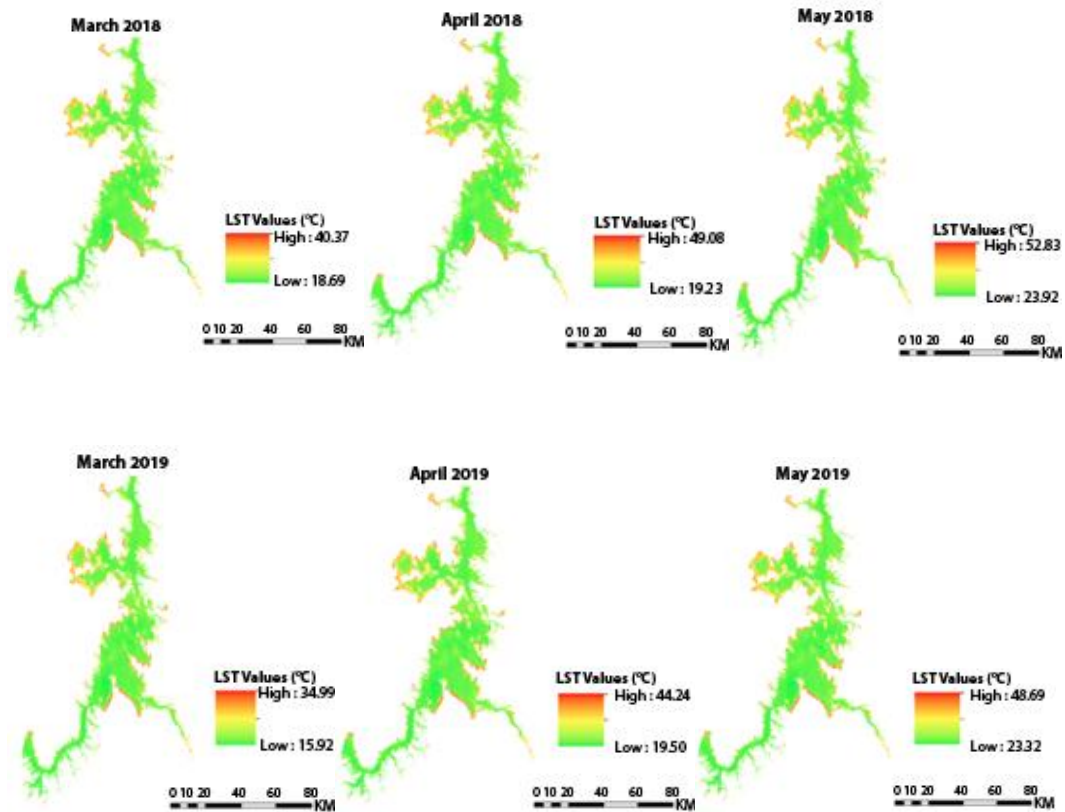
## **3-Results and Discussion**

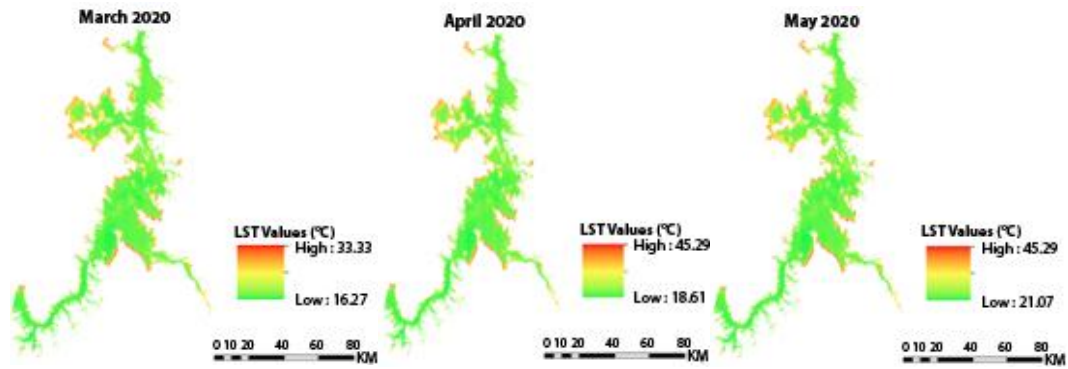
### **3.1 Results of the Estimation of the surface temperature from Landsat-8 images**

The inverse of Planck's function was used to estimate the surface temperature values using Landsat 8 images (the reference values), which is one of the most accurate techniques known to determine temperature values. The deduced surface water temperature maps for the study area are shown in Figure 3. Moreover, the prevailing (most frequent) WST values in the study area estimated by Landsat 8 images are illustrated in Table 3.

**Table 3.** The prevailing LSWT values estimated by Landsat-8 satellite images.

Month	Prevailing Temperature Values °C (Landsat-8)
March 2018	22.65
April 2018	25.53
May 2018	32.19
March 2019	23.04
April 2019	26.97
May 2019	28.93
March 2020	22.18
April 2020	26.89
May 2020	26.75



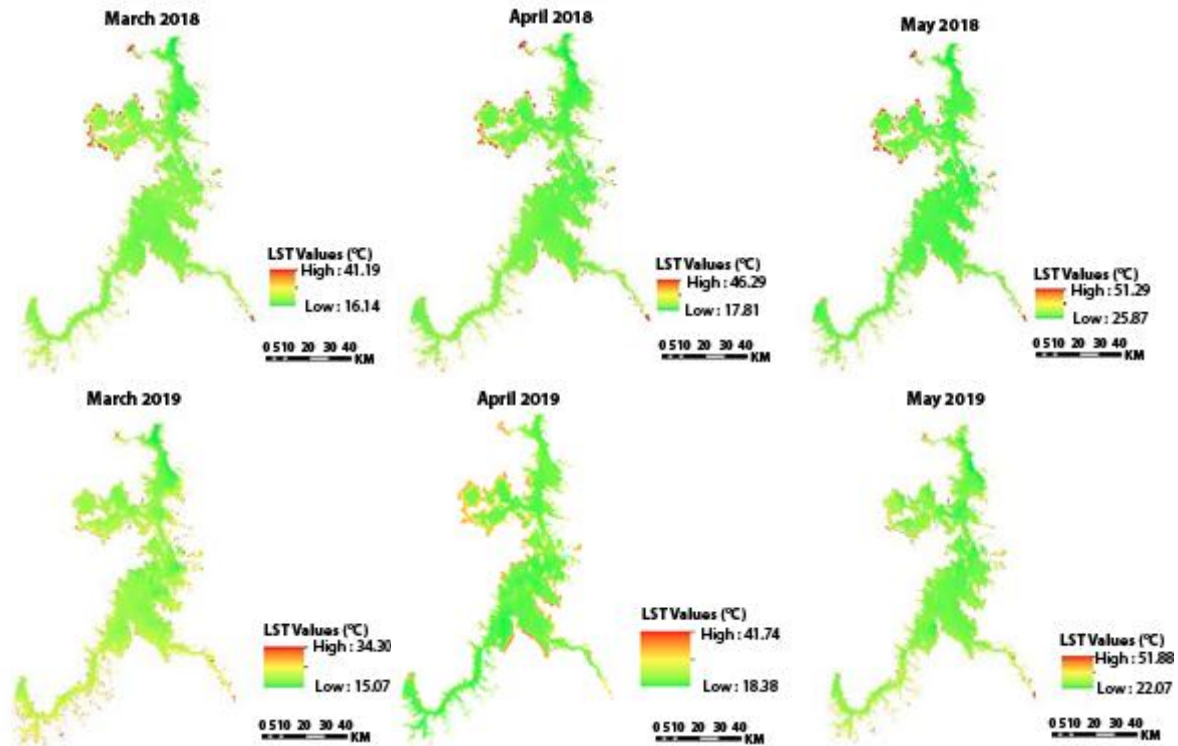


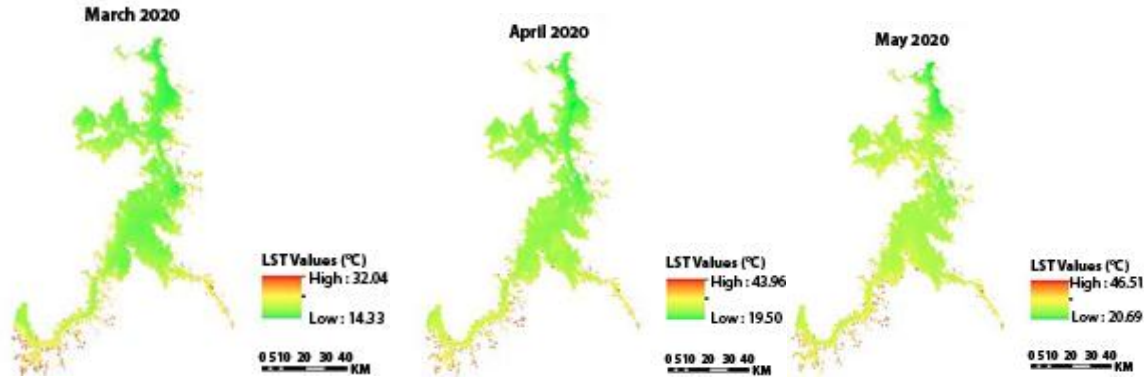
**Fig. 3** The Lake Surface Water Temperature layers was obtained by Landsat-8 satellite images

Table 3 and Figure 3 show that the temperatures reaching their highest values in May every year. The year 2018 saw high temperatures. The following years saw a drop in temperatures values. These results points to a possible downward trend over these three years especially noticeable in the peak May temperatures.

### 3.2 Results of the Estimation of LSWT from Sentinel-3/SLSTR images

The derived LSWT maps by Sentinel-3/SLSTR images are shown in Figure 4. Moreover, the obtained prevailing values of LSWT within the study area using the same satellite images are indicated in Table 4.





**Fig. 4** The Lake Surface Water Temperature maps derived from Sentinel-3/SLSTR satellite images

**Table 4.** The prevailing LSWT values estimated by Sentinel-3/SLSTR satellite images.

Month	Prevailing Temperature Values °C
March 2018	23.11
April 2018	24.52
May 2018	31.43
March 2019	22.62
April 2019	25.70
May 2019	29.22
March 2020	21.42
April 2020	26.23
May 2020	27.34

From Figure 4 and Table 4, which illustrate the results of the study and depict the spatial distribution of the surface water temperature of AHDL, the following can be observed: the lake water temperature varies throughout the studied months, with the highest temperatures recorded during the months of May in all studied years. The lake surface water recorded its lowest temperatures during the months of March. This can be attributed to thermal storage processes due to differences in the depth of the lake.

#### Comparison of the Estimated Lake Surface Water Temperatures.

The accuracy of the estimated LSWT values by Sentinel-3/SLSTR satellite images was assessed by comparing them with the estimated LSWT values by Landsat-8 images. The comparison between the estimated temperature values by both satellite images is summarized in Table 5.

Table 5 presents the comparative analysis of temperature values derived from Sentinel-3/SLSTR satellite images and those calculated using the inverse of Planck's function from 8 Landsat images. These variations could be attributed to differences in sensor calibration, atmospheric conditions, or surface emissivity between the two satellite systems. Overall, the trend of temperature shows good consistency with some discrepancies that are probably because of the intrinsic differences within the satellite sensors and their processing algorithms for data obtained. The estimated temperature values using Sentinel-3/SLSTR satellite images differ by

1.00% to 4.71% from the values of the reference. This small variation range confirms that Sentinel-3/SLSTR satellite imagery is reliable for surface temperature value estimation within the AHDL.

**Table 5.** The comparison between the LSWT values obtained from Sentinel-3/SLSTR satellite images and those obtained from Landsat-8 satellite images.

Month	Temperature(°C) (Sentinel-3/SLSTR)	Temperature(°C) (Landsat-8)	% difference
March 2018	23.11	22.65	2.03%
April 2018	24.52	25.53	-3.96%
May 2018	31.43	32.19	-2.36%
March 2019	22.62	23.04	-1.82%
April 2019	25.70	26.97	-4.71%
May 2019	29.22	28.93	1.00%
March 2020	21.42	22.18	-3.43%
April 2020	26.23	26.89	-2.45%
May 2020	27.34	26.75	2.21%

### 3.3 Relationship between Evaporation Rate and LSWT.

The authors further relate the evaporation rate to the LSWT derived from Sentinel-3/SLSTR satellite images to gain insights into the reasons for these changes in evaporation rate. This will be able to provide an understanding of the basic mechanism underlying these variations in evaporation.

**Table 6.** The evaporation rates and corresponding water surface temperature.

Month	Evaporation rate (mm/month)	Temperature (°C)
March 2018	156.44	23.11
April 2018	178.73	24.52
May 2018	216.10	31.43
March 2019	153.31	22.62
April 2019	217.32	25.70
May 2019	245.60	29.22
March 2020	153.12	21.42
April 2020	245.32	26.23
May 2020	248.20	27.34

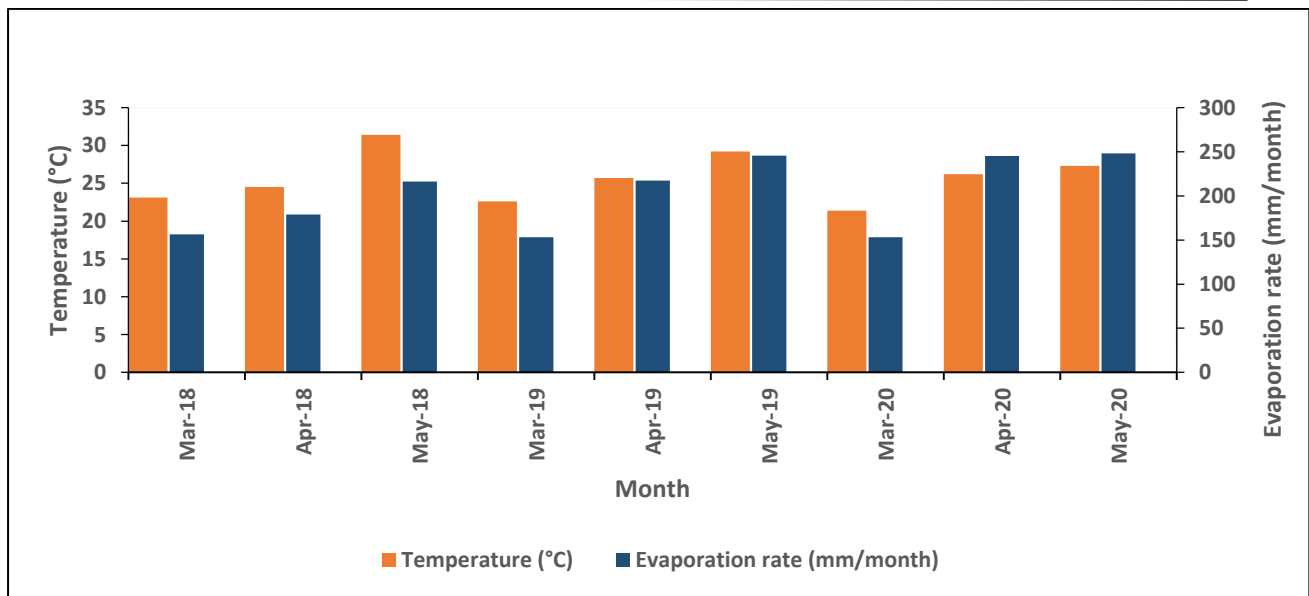


**Fig. 5** Variation of evaporation rate related to surface water temperature from March to May during the years of study

From Table 6 and Figure 5, it can be seen that the rate of evaporation increases with higher temperatures. The evaporation and temperatures for the year 2018 were less compared to the other years, whereas in May 2018, the maximum recorded values were 216.10 mm/month and 31.4°C, respectively. In the year 2019, the rates of evaporation and temperature also went up during April and May, recording 245.60 mm/month and 29.2°C in May 2019. This was also the case in 2020, with April and May showing steep increases, peaking at 248.20 mm/month in May 2020 for a temperature of 27.3°C. These point to a trend whereby there exists a great relation between increased temperatures and increased evaporation rates. That is, evaporation rates show a direct relationship with LSWT within the same year; these rates do change each year due to different annual temperatures. This fluctuation annually proved that there are additional factors affect the evaporation rate.

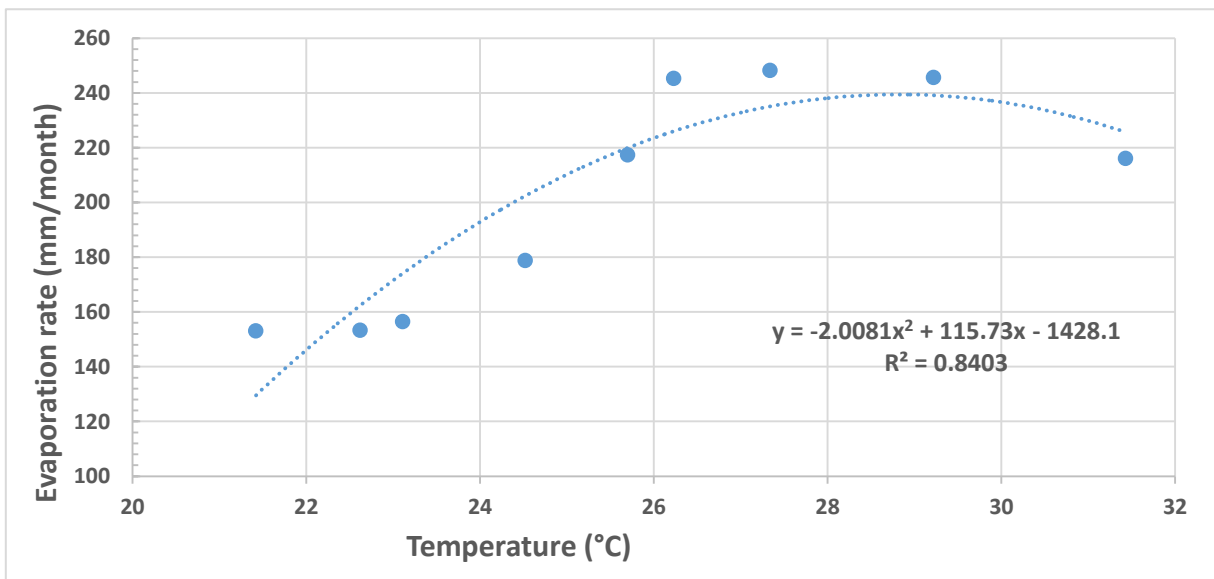


**Fig. 6** Relationship between the evaporation rate and surface water temperature

Figure 6 presents a relationship between evaporation rate (mm/month) and temperature (°C), revealing a complex interaction between these two variables. The fitted curve in the graph is a polynomial of the second degree (quadratic), represented by the equation:

$$(y = -2.0081x^2 + 115.73x - 1428.1) \quad (7)$$

Where:

y: Evaporation rate

x: temperature

This equation effectively captures the initial increase in evaporation rate with rising temperatures, followed by a decrease as temperatures continue to rise. Such behavior is critical for understanding the dynamics of evaporation, particularly in various environmental contexts. The coefficient of determination ( $R^2 = 0.8403$ ) indicates that approximately 84% of the variability in evaporation rate can be explained by temperature. This relatively strong fit suggests that temperature is a significant predictor of evaporation rate, although the remaining 16% of variability may be influenced by other factors. These factors may include wind speed, humidity, the amount of solar radiation, air pressure, and generally the climatic condition. For an overall understanding, more analysis would have to be done considering these additional variables.

#### 4 - CONCLUSION

The primary objective of this research is to estimate the water surface temperature values in the AHDL using Sentinel-3/SLSTR satellite images within the years 2018, 2019 and 2020. The inverse of Planck's function, based on Landsat-8 images, was used to calculate the reference LSWT values. A comparison between temperature values from Sentinel-3/SLSTR and reference values revealed the convergent between them as the convergence percent ranged from 1.00% to 4.71%. These results proved that Sentinel-3/SLSTR satellite images can be reliably used to estimate the surface temperature values in the AHDL. The analysis of the results highlights a significant relationship between temperature and evaporation rate, characterized by a clear polynomial trend. This relationship underscores the importance of considering temperature effects in practical applications related to climate and water management, suggesting pathways for future research to refine our understanding of evaporation processes. Moreover, the results showed that there is a direct relationship between the evaporation rate and LSWT in the same year. However, due to temperature changes from year to year, the evaporation rates fluctuate, hence proving that LSWT is not the only influencing factor on the evaporation rate within the lake. Other factors affecting the evaporation rate in AHDL should be targeted in future studies. Integration of results from those future studies and the present study will be very useful for management of AHDL.

#### References

- Abou El-Magd, I. H., & Ali, E. M. (2012). Estimation of the evaporative losses from Lake Nasser, Egypt using optical satellite imagery. *International Journal of Digital Earth*, 5(2), 133-146.
- Agrama, A. A. (2011). Assessment of climate changes impacts on Lake Nasser water quality. *African J. Biol. Sci*, 7(2), 147-162.

- Alcântara, E. H., Stech, J. L., Lorenzetti, J. A., Bonnet, M. P., Casamitjana, X., Assireu, A. T., & de Moraes Novo, E. M. L. (2010). Remote sensing of water surface temperature and heat flux over a tropical hydroelectric reservoir. *Remote Sensing of Environment*, 114(11), 2651-2665.
- Bates, B, Kundzewicz, Z, Palutikof, J, et al., (2008). Climate Change and Technical Paper of the Intergovernmental Panel on Climate Change (IPCC). Technical paper VI, IPCC Secretariat, 214p.
- Chang, Y., & Li, D. (1996). Normal approach to the linearized Fokker-Planck equation for the inverse-square force. *Physical Review E*, 53(4), 3999.
- Choung, Y. J., Chung, Y. I., & Choi, S. Y. (2018). Assessment of the relationship between air temperature and TOA brightness temperature in different seasons using Landsat-8 TIRS. *Journal of the Korean Association of Geographic Information Studies*, 21(2), 68-79.
- Ebaid, H. M., & Ismail, S. S. (2010). Lake Nasser evaporation reduction study. *Journal of advanced research*, 1(4), 315-322.
- El Moattassem, M., Rafik, M., Makary, A., Heikal, M. T., & Ramadan, A. (1993). Review of Aswan High Dam Lake water quality. In *International symposium on High Aswan Dam: vital achievements, fully controlled Cairo, Egypt*.
- Elba, E., Urban, B., Ettmer, B., & Farghaly, D. (2017). Mitigating the impact of climate change by reducing evaporation losses: sediment removal from the High Aswan Dam reservoir. *American Journal of Climate Change*, 6(02), 230.
- EL-Mekawy, M. I., Ismail, A., & Abdelkhalek, A. (2018). The impact of lake water surface temperature on evaporation from the Aswan High Dam Lake. *Environmental Monitoring and Assessment*, 190(6), 362. <https://doi.org/10.1007/s10661-018-6709-8>
- Elsawwaf, M., Willems, P., Pagano, A., & Berlamont, J. (2010). Evaporation estimates from Nasser Lake, Egypt, based on three floating station data and Bowen ratio energy budget. *Theoretical and applied climatology*, 100, 439-465.
- Estévez, J., Berger, K., Vicent, J., Rivera-Caicedo, J. P., Woher, M., & Verrelst, J. (2021). Top-of-atmosphere retrieval of multiple crop traits using variational heteroscedastic Gaussian processes within a hybrid workflow. *Remote sensing*, 13(8), 1589.
- Garcia, D. H. (2021). Analysis and precision of the Terrestrial Surface Temperature using Landsat 8 and Sentinel-3/SLSTR images: Study applied to the city of Granada (Spain). *Sustainable Cities and Society*, 71, 102980.
- Gianniou, S. K., & Antonopoulos, V. Z. (2007). Evaporation and energy budget in Lake Vegoritis, Greece. *Journal of Hydrology*, 345(3-4), 212-223.
- Hassan, M. (2013). Evaporation estimation for Lake Nasser based on remote sensing technology. *Ain Shams engineering journal*, 4(4), 593-604.
- Huang, S., Tang, L., Hupy, J. P., Wang, Y., & Shao, G. (2021). A commentary review on the use of normalized difference vegetation index (NDVI) in the era of popular remote sensing. *Journal of Forestry Research*, 32(1), 1-6.
- Kong, X., Li, Y., Wang, L., & Liu, H. (2024). Lake Surface Temperature Retrieval Study Based on Landsat 8 Satellite Imagery—A Case Study of Poyang Lake. *Atmosphere*, 15(4), 428.
- Langer, M., Westermann, S., & Boike, J. (2010). Spatial and temporal variations of summer

- surface temperatures of wet polygonal tundra in Siberia-implications for MODIS LST based permafrost monitoring. *Remote Sensing of Environment*, 114(9), 2059-2069.
- Layden, A., Merchant, C., & MacCallum, S. (2015). Global climatology of surface water temperatures of large lakes by remote sensing. *International Journal of Climatology*, 35(15), 4464-4479.
- Lazhu, Yang, K., Wang, J., Lei, Y., Chen, Y., Zhu, L., & Qin, J. (2016). Quantifying evaporation and its decadal change for Lake Nam Co, central Tibetan Plateau. *Journal of Geophysical Research: Atmospheres*, 121(13), 7578-7591.
- Lenters, J. D., Kratz, T. K., & Bowser, C. J. (2005). Effects of climate variability on lake evaporation: Results from a long-term energy budget study of Sparkling Lake, northern Wisconsin (USA). *Journal of Hydrology*, 308(1-4), 168-195.
- Meng, X., Liu, H., Du, Q., Xu, L., & Liu, Y. (2020). Evaluation of the performance of different methods for estimating evaporation over a highland open freshwater lake in mountainous area. *Water*, 12(12), 3491.
- MWRI (2022). The Ministry of Water Resources and Irrigation, Egypt, “Annual report (2018- 2022),” Nile Water Sector.
- Obertegger, U., & Flaim, G. (2021). A 40-year perspective of an alpine lake: Is everything the same? *Limnologica*, 91, 125929.
- Oesch, D., Jaquet, J. M., Klaus, R., & Schenker, P. (2008). Multi- scale thermal pattern monitoring of a large lake (Lake Geneva) using a multi- sensor approach. *International Journal of Remote Sensing*, 29(20), 5785-5808.
- Omran, E. S. E., & Negm, A. (2019). Environmental impacts of the GERD project on Egypt’s Aswan high dam lake and mitigation and adaptation options. *Grand Ethiopian renaissance dam versus Aswan high dam: a view from Egypt*, 175-196.
- Reinart, A., and Reinhold, M. (2008). Mapping surface temperature in large lakes with MODIS data. *Remote Sensing of Environment*, 112(2), 603-611.
- Steissberg, T. E., Hook, S. J., & Schladow, S. G. (2005). Characterizing partial upwellings and surface circulation at Lake Tahoe, California–Nevada, USA with thermal infrared images. *Remote sensing of environment*, 99(1-2), 2-15.
- Xiao, W., Zhang, Z., Wang, W., Zhang, M., Liu, Q., Hu, Y., & Lee, X. (2020). Radiation controls the interannual variability of evaporation of a subtropical lake. *Journal of Geophysical Research: Atmospheres*, 125(8), e2019JD031264.
- Xu, R., Pan, Z., Han, Y., Zheng, W., & Wu, S. (2023). Surface Properties of Global Land Surface Microwave Emissivity Derived from FY-3D/MWRI Measurements. *Sensors*, 23(12), 5534.
- Zhao, Q., & Qu, Y. (2024). The Retrieval of Ground NDVI (Normalized Difference Vegetation Index) Data Consistent with Remote-Sensing Observations. *Remote Sensing*, 16(7), 1212.
- Zhu, S., Ptak, M., Yaseen, Z. M., Dai, J., & Sivakumar, B. (2020). Forecasting surface water temperature in lakes: A comparison of approaches. *Journal of hydrology*, 58